Biosensors and Bioelectronics 74 (2015) 341–346

Contents lists available at ScienceDirect

Biosensors and Bioelectronics

journal homepage: www.elsevier.com/locate/bios

A nanoplasmonic biosensor for label-free multiplex detection of cancer biomarkers

Jong Uk Lee [a], Anh H. Nguyen [a], Sang Jun Sim [a,b,*]

[a] Department of Chemical and Biological Engineering, Korea University, Seoul 136-713, Republic of Korea
[b] Green School, Korea University, Seoul 136-713, Republic of Korea

ARTICLE INFO

Article history:
Received 27 April 2015
Received in revised form
22 June 2015
Accepted 25 June 2015
Available online 30 June 2015

Keywords:
Localized surface plasmon resonance
Multiplex detection
Gold nanoparticles
Cancer biomarkers

ABSTRACT

The development of highly sensitive, selective and multiplex sensors has become an important challenge for disease diagnosis. In this study, we describe a multiplex biosensor for the detection of cancer biomarkers based on unique plasmon response of single gold nanoparticles (AuNPs) and antibody–antigen binding activity. To demonstrate the ability of the plasmon biosensor to detect and quantify cancer biomarkers: a panel of biomarkers, including α-fetoprotein (AFP), carcinoembryonic antigen (CEA) and prostate specific antigen (PSA) was used as a model analyte for multiple detection. A novel and sensitive multiplex biosensor was developed by immobilizing plasmonic nanoparticles in a site-specific manner and functionalized with monoclonal antibodies that recognize the target protein on hydrophilic–hydrophobic patterned glass slide. The proposed multi-analyte biosensor exhibited outstanding selectivity and sensitivity. The limit of detection was determined to be 91 fM, 94 fM and 10 fM for AFP, CEA and PSA from patient-mimicked serum, respectively. Finally, using this sensing strategy, this platform presents an excellent approach for versatile molecular diagnostics in both research and clinical medical fields.

1. Introduction

Cancer is a major cause of death worldwide. Approximately 14 million new cases and 8.2 million cancer-related death were reported in 2012, and annual number of cancer-related deaths continues to rise (Coleman, 2014). According to the report of World Health Organization, if case of cancer resulting in death were detected and treated at early stage, more than 30% of these death could be avoided (Ilbawi et al., 2015). Therefore, the detection of cancer biomarkers at the early stage has attracted considerable attention in the field of clinical diagnosis because it is useful for evaluating the extent of cancer, monitoring the response of cancers to therapy, and predicting recurrence (Maruvada et al., 2005).

In life science, immunoassay and immunosensor for a single cancer biomarker have yet to be developed (Wang et al., 2009; Jie et al., 2011). Approaches used in cancer diagnosis should be rapid, sensitive, highly reproducible, and reliable (Liu et al., 2009; Zhan et al., 2012; Xue et al., 2013; Zhao et al., 2013). Among the current methods for cancer biomarker detection, the plasmonic biosensor platform is one of powerful tools for clinical diagnostics and has recently attracted considerable attention, because it contributes many promising functions, such as high selectivity and, sensitivity, as well as real time and label-free detection (Haes et al., 2004; Rosi and Mirkin, 2005; Gish et al., 2007; Song et al., 2013). The plasmonic biosensor detects the incident photon frequency generated by the collective coherent oscillation of the free electrons surrounding nanometer-sized metallic nanoparticle (e.g., AuNPs) under the electromagnetic field of incoming light. This results in Rayleigh light scattering, which is also called localized surface plasmon resonance (LSPR) (McFarland and Van Duyne, 2003; Liu et al., 2006; Anker et al., 2008). The resonance wavelength at the surface of nanoparticle (LSPR) is dependent on the shape, size, and the dielectric environment surrounding the AuNPs (Truong et al., 2014). For this reason, nanoplasmonic biosensors have the potential to serve as platform for detecting biological molecules and biochemical binding events occurring on the nanoparticle surface due to changes in the local refractive index (Huang et al., 2009).

As reported in previous studies, our group has developed an individual nanoplasmonic platform for detecting cancer biomarkers (Cao and Sim, 2007; Truong et al., 2011; Hwang et al., 2012; Jun et al., 2014). Nanoplasmonic biosensors based on a single gold particle have a sensing concentration in the attomolar range, which is well suited for detection of a single biomarker. Moreover, the diagnostic power is increased when a panel of biomarkers can be monitored simultaneously in one device. However, the measurement of a single cancer biomarker is not sufficient for cancer diagnosis due to the heterogeneous nature of

* Corresponding author.
E-mail address: simsj@korea.ac.kr (S.J. Sim).

http://dx.doi.org/10.1016/j.bios.2015.06.059
0956-5663/

cancer genetics; most cancers are associated with more than one biomarker (Niklinski and Furman, 1995; Gregory Jr and Finlay, 1999). Panels of cancer biomarkers may provide abundant analytical and diagnostic information and improve diagnostic value by streamlining the procedure to one multiplex plasmonic sensor, thereby creating an urgent demand for enhanced detection throughput and multiple detection platforms (Zhan et al., 2012). Multiple detection platforms should be capable to rapid, sensitive, and simultaneous detection that also analyze multiple analytes in a single sample. In addition, it would result in ideally shorten analytical time, increased throughput detection and lower costs (Barbee et al., 2010).

In the present study, we propose a nanoplasmonic biosensor platform for multiple label-free detection of cancer biomarkers to achieve highly selective and sensitive detection of target biomarkers using site-selectively immobilized gold nanoparticles on the hydrophilic–hydrophobic patterned glass. The detection of target binding activity was monitored via spectral changes caused by a change in the local refractive index of vicinity of individual nanoparticles. As proof of concept, we used AFP, CEA, and PSA as model analytes in the proposed method to demonstrate good analytical performance. The detection limits of the platform were determined to be 91 fM, 94 fM and 10 fM for AFP, CEA and PSA from patient-mimicked serum. We anticipate that multiple label-free nanoplasmonic biosensor, as described herein, will be suitable for the detection of cancer biomarkers. This platform also provides a powerful tool that, when developed, will be a rapid, low-cost, high throughput bioprocess biosensor.

2. Materials and methods

2.1. Materials

Hydrogen tetrachloroaurate(III) trihydrate ($HAuCl_4 \cdot 3H_2O$), 1-ethyl-3-(3-dimethylaminopropyl) carbodiimide (EDC), N-hydroxysuccinimide (NHS), phosphate buffer saline pH 7.4 (PBS buffer), 3-aminopropyltriethoxysilane (APTES), bovine serum albumin (BSA), trichloro(octadecyl) silane (OTS), sulfuric acid (H_2SO_4), hydrogen peroxide (H_2O_2), nitric acid (HNO_3), 2-aminoethanethiol and human serum were purchased from Sigma-Aldrich, Inc. (St. Louis, MO, USA). Sodium borohydride ($NaBH_4$) was purchased from Fluka Analytical (Missouri, USA). AFP monoclonal antibody (AFP-mAb), CEA monoclonal antibody (CEA-mAb), PSA–ACT complex monoclonal antibody (PSA-mAb), AFP protein, CEA protein, and PSA–ACT complex protein were supplied by Fitzgerald Industries International, Inc. (Acton, MA, USA). Acetone, ethanol, methanol, and n-hexane were purchased from Samchun Chemical Co. (Gyeonggi-Do, Korea). Coverslip slides ($22 \times 40 \times 0.1$ mm^3) were purchased from Deckglaser (Germany). Other essential reagents were supplied by Sigma Aldrich Inc. The sylgard 184 silicone elastomer kit was purchased from Dow Corning (Michigan, USA) and was used to fabricate poly(dimethylsiloxane) (PDMS) stamps. Ultra-pure water (18.2 mΩ cm^{-1}), purified by reverse-osmosis, was used to prepare all chemical solutions. All glassware used in the experiments was cleaned in freshly prepared aqua regia solution and rinsed thoroughly in ultra-pure water before use.

2.2. Amino-modified gold nanoparticles synthesis

Amino-modified gold nanoparticles were synthesized in aqueous solution by sodium borohydride reduction, following a previously published protocol with some modifications (Niidome et al., 2004; Wang et al., 2012). An HAuCl4 solution (290 μL, 100 mM) was diluted with water (79.71 mL), and a 2-aminoethanethiol solution (170 μL, 213 mM) was added to the gold solution. After stirring for 20 min at room temperature, $NaBH_4$ solution (4.2 μL, 18 mM) was added, and the mixture was stirred for more than 10 h in the dark. Then, the solution was filtered through a 0.2 μm filter to remove any aggregated particles and was characterized using a UV/vis spectrometer (Shimadzu UV-3600, Kyoto, Japan). The colloidal solution was subsequently centrifuged at 7000 rpm for 15 min to separate unbound 2-aminoethanethiol. The sediment was re-suspended in ultra-pure water and stored at 4 °C until further use. The size and the homogeneity of AuNPs were determined by high-resolution transmission electron microscopy (HR-TEM) conducted on a JEM3010 instrument operating at a voltage of 300 kV. The final solution was stored at 4–8 °C in refrigerator.

2.3. Preparation of immuno-gold nanoparticles

For preparation of immuno-gold nanoparticles, 500 μL of each target protein monoclonal antibody (mAb) (1 mg mL^{-1}) was mixed with EDC/NHS (1 M, 10 μL) to convert the carboxyl groups of the C-terminal Fc region of antibodies to NHS esters in order to prepare the immuno-gold colloids. After 15 min, 1 mL of the stabilized AuNPs ($A_{535} \approx 2$) was added to activate each target protein. The solution was mixed well and incubated at room temperature for 1 h. Then, the immuno-gold nanoparticles were centrifuged at 5000 rpm for 15 min, the supernatant was discarded, and the sediment was re-dispersed in 0.01 M PBS buffer (pH 7.4) and stored at 4 °C until further experimentation.

2.4. Fabrication of PDMS stamp

PDMS stamps with 3 defined holes (2 mm in diameter) were designed with AutoCAD software (Autodesk, USA) and printed on transparency photomask film (Han & All Technology, Korea). Briefly, silicone elastomer base and curing agent were thoroughly mixed in a 10:1 ratio and degassed for 1 h before pouring into a pre-casted mold. Curing was carried out at 80 °C for 4 h. The cured PDMS sheet with a thickness of 2 cm was carefully detached from the mold after cooling to room temperature and cut into pre-designed patterns.

2.5. Preparation of hydrophilic–hydrophobic patterned glass slides and immuno-AuNPs immobilization

Microscopic glass slides ($22 \times 40 \times 0.1$ mm^3) from Warner Instruments were cleaned overnight using freshly prepared aqua regia solution and then thoroughly rinsed with ultrapure water. Briefly, the cleaned glass slides were dipped in 1% (v/v) trichloro (octadecyl)silane (OTS) in n-hexane for 15 min. To remove excess OTS, glass slides were rinsed with ethanol three times before drying at 60 °C for another 4 h. To fabricate hydrophilic–hydrophobic patterned glass slides, a pre-designed PDMS stamp was compressed onto OTS-treated glass and exposed to oxygen plasma at 80 W for 9 s to locally convert the terminal groups of the OTS in exposed regions to hydroxyl groups (Lin et al., 2009). The site-selectively modified glass slide was dipped in 5% (v/v) APTES in 99.9% ethanol for 15 min. Then, the glass slides were sonicated in ultrapure water three times for 5 min. Therefore, the hydrophilic regions treated with O_2 plasma were functionalized by APTES to expose amino groups, while the other regions maintained the hydrophobic characteristics of OTS. After the washing step, silanization was completed by drying the slides at 120 °C for 2 h. Immuno-AuNPs were randomly immobilized onto a silanized glass slide by drop-coating 10 μL of the diluted AuNP solutions ($OD_{520} \approx 0.04$) onto the center of the predesigned holes and incubating for 1 min to determine the optical response of individual

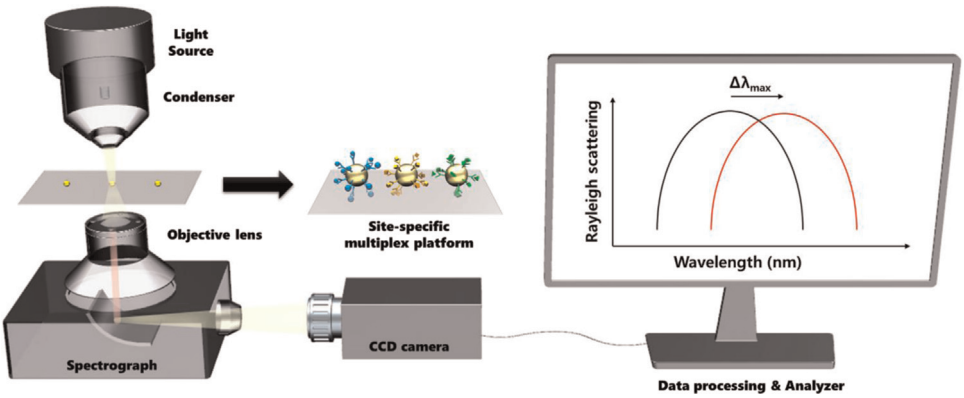

Fig. 1. Schematic illustration of the fabrication of plasmonic biosensor for multiple label-free cancer biomarker detection.

AuNPs. After incubation, the slides were washed with ultrapure water and ethanol and dried with nitrogen gas. The immuno-AuNP-immobilized slide was mounted in an RC-30 closed-bath imaging chamber. The imaging chamber was assembled onto the sample holder of a dark-field microscope and was connected with a syringe pump (Harvard Apparatus, Holliston, MA, USA), and the surface was covered with the 5 μL sample solution. Finally, the resonant Rayleigh light-scattering spectra of representative single AuNPs were recorded.

2.6. Dark-field microscopy

Single-particle measurement is a unique strategy for sensing a single nanoparticle by dark-field microscopy in combination with spectrophotometry (Fig. 1). The details of this system have been described previously (Song et al., 2013; Truong et al., 2014). Briefly, the spectral measurement was carried out using an inverted microscope (Eclipse TE2000-U, Nikon, Tokyo, Japan) equipped with a dark-field condenser (dry condenser, NA=0.80–0.95, Nikon), a 100 W tungsten lamp, a digital camera (D50, Nikon), and a spectrograph (Microspec 2300i, Roper Scientific, Tuscon, Arizona, USA) equipped with a highly sensitive CCD camera (PIXIS: 400B, Roper Scientific). True-color scattering images were taken using a 100 × objective (CFI Plan Fluor ELWD, NA=0.6). The scattered monochromatic light was recorded with the CCD camera and plotted as a function of light-scattering intensity versus wavelength. To reduce the noise from ambient light, the microspectroscopy system was completely covered by a dark shield.

2.7. Target cancer biomarkers detection based on an individual immuno-AuNP

After settling the imaging chamber and the optical system, the overall experimental process involving individual immuno-nanoparticle sensors proceeded as described below (Fig. 1). First, the surface of a glass slide was washed with de-ionized water for 30 min to remove all contaminants and unbound immuno-AuNPs. Next, a methoxy polyethylene glycol succin-imidyl valerate (mPEG-SVA) solution was injected into the chamber and incubated for 6 h to prevent non-specific binding of target cancer biomarkers to the microscope slide (Waldeisen et al., 2011). Finally, various concentrations of each cancer biomarker, ranging from 1 fM to 1×10^6 fM, were diluted in serum samples and mixed. These antigen mixtures were flowed over the immuno-AuNP surface inside the flow cell and incubated for 1 h. The surface of a glass slide was rinsed by injecting distilled water over the flow cell for 5 min after every chemical binding step, and the resonant λ_{max} shift induced by analyte binding was recorded by measuring the scattering spectra of an individual immuno-AuNP. The Lorentzian algorithm was employed to fit the spectra and to identify accurate peaks using OriginPro 8.0 software. The change in the refractive index corresponding to each molecular binding step on the nanoparticle surface was observed and expressed as an LSPR $\Delta\lambda_{max}$ shift. The LSPR λ_{max} shift was calculated as follows: $\Delta\lambda_{max}=\lambda_{max}$ (after chemical binding) $-\lambda_{max}$ (before chemical binding).

3. Results and discussion

3.1. Synthesis of immuno-gold nanoparticle

We synthesized 50 nm amino-modified gold nanoparticles following previously reported methods (Niidome et al., 2004; Sharmaa et al., 2010; Wang et al., 2012). We directly confirmed synthesized 50-nm amino-gold nanoparticles using a TEM image (Fig. 2A), and FT-IR spectra (Fig. 2B). The FT-IR spectra of amino-gold nanoparticles showed that $-NH_2$ stretch was a broad bend ranging from 3300 to 3500 cm^{-1}. The broad absorption bands near 3300 cm^{-1} could be assigned to primary amines (Singh et al., 2006; Sharmaa et al., 2010; Zhang et al., 2009). Furthermore, it is well known that 2-aminoethanethiol is frequently used both as a linking agent and as a stabilizer for gold nanoparticles. Here, the SH (sulfur) group of 2-aminoethanethiol are used to bind the surface of gold nanoparticles, NH_2 (amino) group of 2-aminoehanethiol are applied for attachment of target cancer biomarker monoclonal antibody to make the immuno-gold nanoparticles (Duan et al., 2010). Fig. 2C (Fig. S1) shows the UV–vis spectrum of the gold nanoparticles after each step (UV–vis spectrum of all case are shown in Fig.S1). This information provided the plasmon resonance characteristics of the gold nanoparticles. The wavelength shifted from 535 nm to 539 nm, corresponding to amino-modified gold nanoparticle and mAb-conjugated gold nanoparticles (immuno-gold nanoparticle), respectively. These results indicate that gold nanoparticle were successfully conjugated with the monoclonal antibody (mAb) via amide bonds. The immunogolds are now ready for capturing target antigens for biosensing, indicating the successful attachment of the target protein layer onto the surface of gold nanoparticles (Truong et al., 2011; Nguyen et al., 2015).

3.2. Fabrication of plasmonic biosensor chip for multiple label-free detection

For multiple label-free detection, a flow-through plasmonic biosensor chip was fabricated on hydrophilic–hydrophobic patterned glass slide via modification of a self-assembled monolayer (SAM) in two steps, using O_2 plasma to improve the target-analyte throughput in combination with a spatially resolved technique as

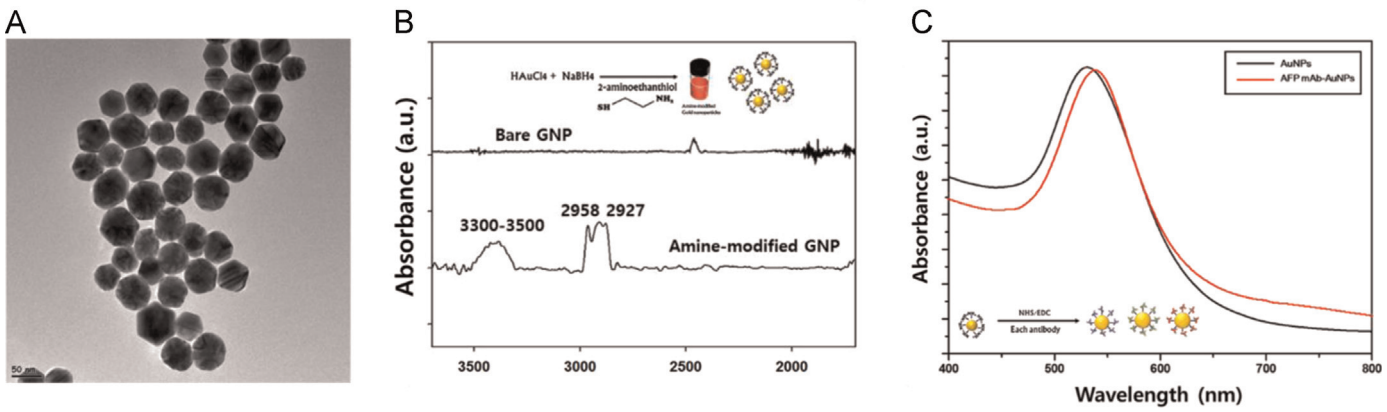

Fig. 2. Immuno-gold nanoparticle synthesis. (A) TEM image of 50 nm AuNPs (B) FT-IR spectra of bare gold nanoparticles and amino-modified gold nanoparticles. The FT-IR spectra of amino-gold nanoparticles showed that $-NH_2$ stretch was broad bend ranging from 3300 to 3500 cm^{-1}. (C) UV–vis spectra of amino-modified gold nanoparticles (AuNPs) (535 nm), and mAb-conjugated AuNPs (539 nm).

shown in Fig 3A (Fu et al., 2006; Wei et al., 2008; Lin et al., 2009). To assess the fabrication of plasmonic biosensor chip step (i.e., to characterize the change of hydrophobic surface to hydrophilic surface), we measured contact angles for a drop of water with the surface of the glass slides after each step (Fig. 2B and Fig. S2). A higher contact angle value indicates the greater hydrophobic property of a surface (Miwa et al., 2000). In experiment, we first treated glass slide with OTS to make the hydrophobic surface via a condensation reaction between silane and hydroxyl moieties. The contact angle with the surface of an OTS-treated glass slide was large as approximately 100°, indicating that the surface became hydrophobic. Second, a site-specific hydrophilic region was achieved in desired regions by O_2 plasma treatment using a PDMS Stamp. PDMS stamps with 3 holes allowed for tight contact with OTS-treated glass slides to form predesigned site-specific hydrophilic regions for O_2 plasma exposure. The contact angle on the O_2 plasma treated surface of glass slide was dramatically reduced, indicating the O_2 plasma treated surface of the glass slide was hydrophilic (Yeo et al., 2006). Based on these results, we fabricated the patterned hydrophilic–hydrophobic surfaces of the plasmonic biosensor chip. To detect multiple label-free cancer biomarkers, a plasmonic biosensor chip was formed upon deposition of the different immuno-gold nanoparticles on the hydrophilic regions of the predesigned glass slide.

3.3. Evaluation of cross-talk on plasmonic biosensor

When the number of target analytes in a multiplex biosensor increases, bottleneck, such as the restriction of available labels, could occur due to cross reactivity (Fu et al., 2006; Wang et al., 2015). To reduce this bottleneck, plasmonic biosensor becomes an option because it has ability to immobilize specific antigen/antibody combinations on the individual surface of a spatially resolved region composed of different target capture antibodies and to

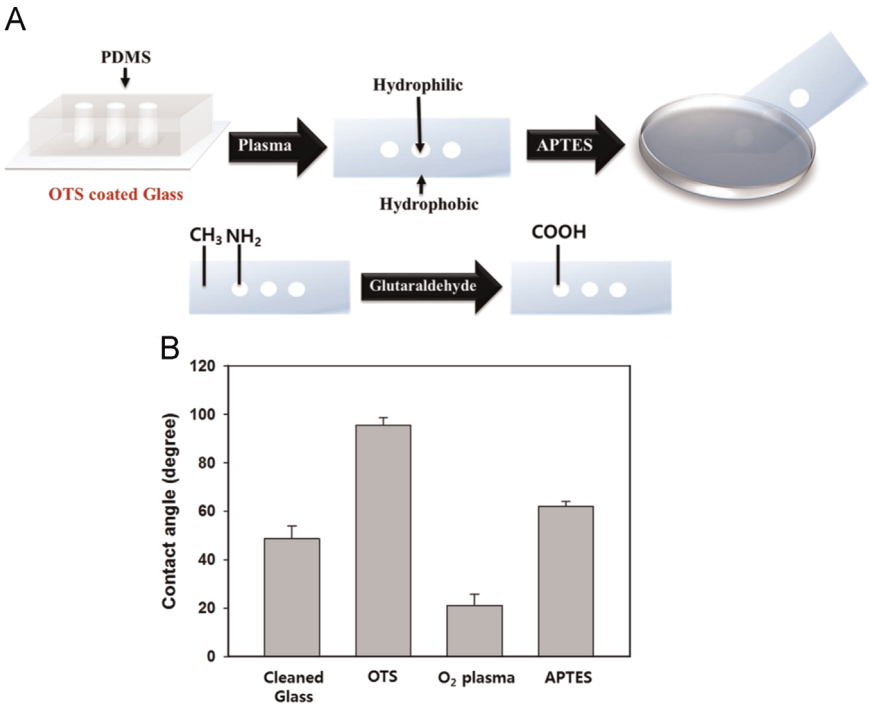

Fig. 3. (A) Schematic illustration of the fabrication of plasmonic biosensor chip for multiple label-free cancer biomarker detection (B) bar graphs for contact angles at each step in the process of construction of the patterned biosensor chip. The data in the bar graph were obtained from at least five independent experiments.

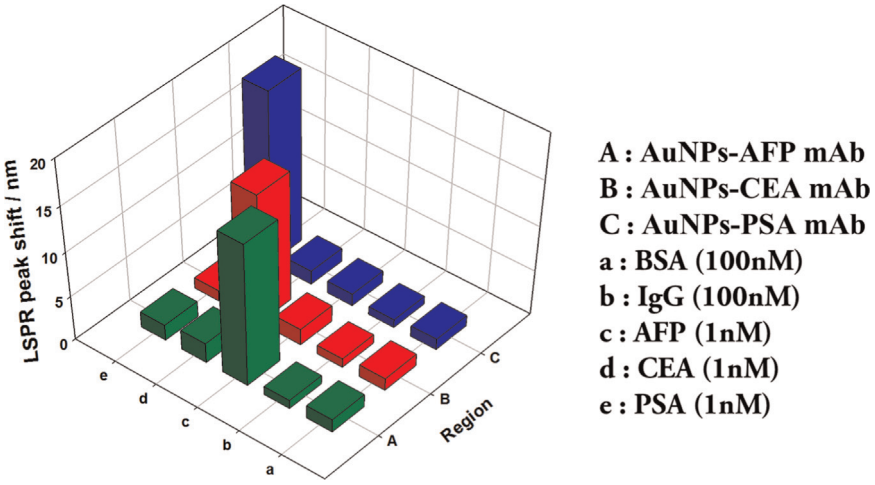

Fig. 4. The LSPR peak shift of site-specific plasmon biosensors for the independent detection of AFP, CEA, and PSA. Regions A, B and C were conjugated with AuNPs-AFP mAb, AuNPs-CEA mAb and AuNPs-PSA mAb, respectively.

recognize different targets using specific binding for identification of cross talk. In this system, three different antibodies for each cancer biomarker were evaluated. In order to distinguish the nonspecific binding from cross talk, BSA and IgG were used. This was because these proteins are ubiquitous in human sample and are well studied for a variety of sensors (Green et al., 1999). Fig. 4 shows the LSPR peak shift of a site-specific plasmon biosensor for the independent detection of AFP, CEA, and PSA. The Rayleigh scattering spectra of each step in the process was recorded. For each target cancer biomarker, only the region containing the AuNPs-cognate target mAb produced a significant LSPR peak shift. Furthermore, in the case of BSA and IgG, even with their concentrations were 100 folds higher than the target protein concentration, no obvious signal changes observed (Fig. 4). The results of treating mixtures of two of the three cancer biomarkers as well as treating a mixture of all three cancer biomarkers are shown in Fig. S3. These results indicated that there was no cross talk between target cancer biomarkers and that nonspecific binding was also negligible. Thus, we confirm that this plasmonic biosensor platform had great selectivity for the detection of the target cancer biomarkers.

3.4. A plasmonic biosensor for multiple label-free detection of three cancer biomarkers

As a demonstration of multiple label-free detection, plasmonic biosensor device were fabricated (Fig. 1). Under the optimal conditions, multiple label-free detection was performed using three cancer biomarkers (AFP, CEA, and PSA) from patient- mimicked serum as model analytes. Analytical performance parameters, such as sensitivity of the plasmonic biosensor platform, were determined for each concentration of cancer biomarkers in the mixture. By analyzing LSPR peak shift based on the concentration of cancer biomarker, we can deduce that LSPR peak shift increased in a manner dependent on the concentration of cancer biomarkers (Fig. 5.A). The LSPR peak shift displayed a strong linear relationship with the concentration logarithm in the range from 10 fM to 10^6 fM (Fig. 5B). The limit of detection (LOD) values of the biosensor were calculated following this formula: (LOD$=3*\delta/m$, where δ is the standard deviation of blank and m is the slope of calibration curve). Calculated values were 91 fM for AFP, 94 fM for CEA, 10 fM for PSA–ACT respectively. The linear regression equations were $y=1.964\log(x)+1.373$ ($R^2=0.996$) for AFP, $y=1.664\log(x)+0.213$ ($R^2=0.913$) for CEA and $y=2.749\log(x)+1.239$ ($R^2=0.987$) for PSA. Using the same method, the experiment was carried out by diluting with PBS (pH 7.4). The corresponding data can be found in Supporting information (Fig. S4). The sensitivity of the plasmonic biosensor platform is suitable for practical and

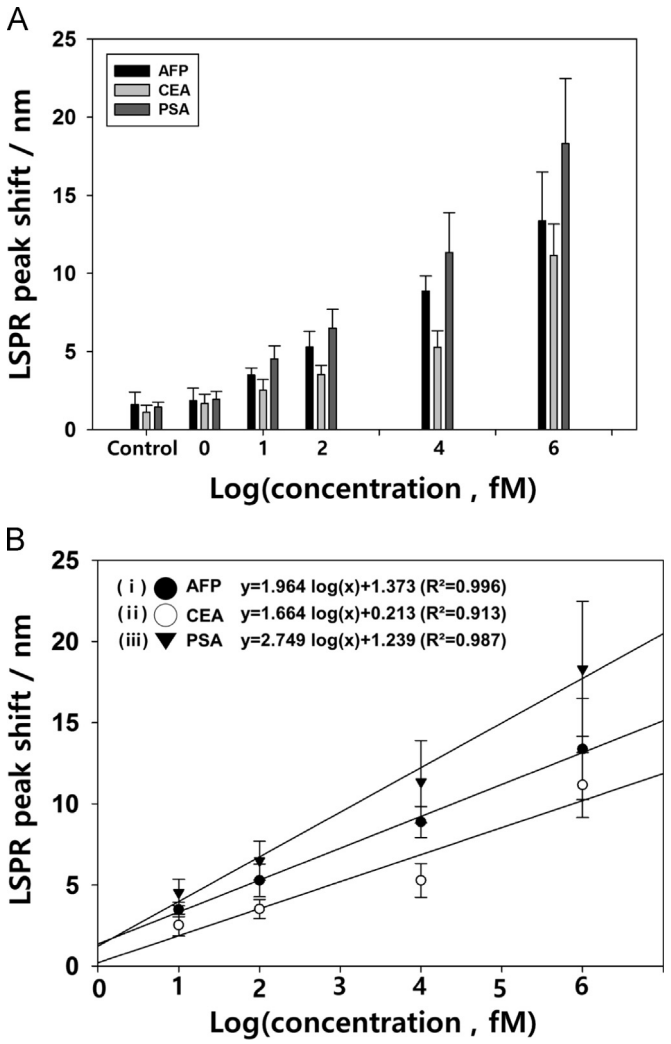

Fig. 5. Detection of AFP, CEA and PSA in patient-mimicked serum. (A) Detection of AFP, CEA and PSA at concentrations ranging from 1 fM to 10^6 fM (B)linear regression of the calibration curve describing the relationship between the LSPR wavelengths peak shifts and AFP. CEA and PSA target cancer biomarker concentrations.

Table 1
Recovery test of AFP, CEA and PSA in the human serum samples.

Samples	AFP	CEA	PSA
Added (ng mL^{-1})	1.0	1.0	1.0
Found (ng mL^{-1})[a]	0.94	0.97	1.08
RSD (%)	6.4	7.0	7.3
Recovery (%)	93.6	97.2	108.2

[a] The average value of three successive determinations.

clinical applications in that the cut off values of the three cancer biomarkers in the diagnostic test were 25 ng/mL (357.14 pM) for AFP, 3 ng/mL (16.67 pM) for CEA and 4 ng/mL (44.44 pM) for PSA (Liu et al., 2009; Zhang et al., 2013). To perform the recovery tests, known amounts of AFP, CEA, and PSA were added into human serum (Sigma Aldrich). The results listed in Table 1 showed recoveries of 93.6%, 97.2%, and 108.2% for AFP, CEA, and PSA, respectively. The RSDs for the three cancer biomarkers were all below 7.3%, demonstrating the adequate accuracy. These results strongly imply that plasmonic biosensor platforms have high potential in clinical tests.

With the significant advances in immunoassay techniques, biosensors for the parallel detection of multiple target biomarkers have been developed using several detection principles such as ELISA (Han et al., 2010), and electrochemistry (Ko et al., 2008). Even though ELISAs provide quantitative detection with high specificity toward an antibiotic, they become laborious and time consuming when lots of samples need to screen. Also, electrochemical techniques such as fluorescent techniques offer higher sensitivities and lower detection limit, however, electrochemical techniques still lack the analytical performance. While our plasmonic biosensor platform is a simple one-step measurement of LSPR peak shift that enables us to detect target molecules and measure the amount of target molecules by analyzing the value of LSPR peak shift. Thus, proposed platform can be a promising candidate for low-cost, label free, highly sensitive and selective detection of multiple target analytes in a rapid and simple format.

4. Conclusions

In this paper, we demonstrate that a nanoplasmonic biosensor platform can be utilized for multiple label-free detection of cancer biomarkers. The proposed plasmonic biosensor was fabricated by site-selectively immobilizing different target immuno-gold nanoparticles on hydrophilic–hydrophobic patterned glass slides, which provides significant advantages, including label-free, highly sensitive, specific and cost-effective detection of target-binding activity between antigens and antibodies. The platform yielded LODs of 91 fM, 94 fM and 10 fM for the model analyse AFP, CEA and PSA from patient-mimicked serum, respectively. This multiple label-free plasmonic biosensor platform can be extended to various cancer biomarkers by using the appropriate bioreceptors or antibodies. Compared with conventional methods, this platform was able to detect cancer biomarkers at a smaller volume and reduce detection time. Based on the results, the plasmonic biosensor described in this paper might have value in a variety fields, including clinical and environmental applications.

Acknowledgments

This study was supported by the National Research Foundation of Korea (NRF) grants (grant No. NRF-2013R1A2A1A01015644/2010-0027955), University-Institute Cooperation Program (2013), and grants (2014M1A8A1049278) from Korea CCS R&D Center of the NRF funded by the Ministry of Science, ICT, & Future Planning of Korea. This study was also supported by the Korea Institute of Energy Technology Evaluation and Planning and Ministry of Trade, Industry & Energy of in “Energy Efficiency & Resources Technology R&D” project Korea (20152010201900).

Appendix A. Supplementary material

Supplementary data associated with this article can be found in the online version at http://dx.doi.org/10.1016/j.bios.2015.06.059

References

Anker, J.N., Hall, W.P., Lyandres, O., Shah, N.C., Zhao, J., Van Duyne, R.P., 2008. Nat. Mater. 7, 442–453.
Barbee, K.D., Hsiao, A.P., Roller, E.E., Huang, X.H., 2010. Lab Chip 10, 3084–3993.
Cao, C., Sim, S.J., 2007. Biosens. Bioelectron. 22, 1874–1880.
Coleman, M.P., 2014. Lancet 383, 564–573.
Duan, R., Zhou, X., Xing, D., 2010. Anal. Chem. 82, 3099–3103.
Fu, Z.F., Liu, H., Ju, H.X., 2006. Anal. Chem. 78, 6999–7005.
Gish, D.A., Nsiah, F., Mcdermott, M.T., Brett, M.J., 2007. Anal. Chem. 79, 4228–4232.
Green, R.J., Davies, M.C., Roberts, C.J., Tendler, S.J.B., 1999. Biomaterials 20, 385–391.
Gregory Jr, J.J., Finlay, J., 1999. Drugs 57, 463–467.
Haes, A.J., Hall, W.P., Chang, L., Klein, W.L., Van Duyne, R.P., 2004. Nano Lett. 4, 1029–1034.
Han, K., Ahn, D., Yang, E.G., 2010. Bioconjugate Chem. 21, 2190–2196.
Huang, H., He, C., Zeng, Y., Xia, X., Yu, X., Yi, P., Chen, Z., 2009. Biosens. Bioelectron. 24, 2255–2259.
Hwang, W.S., Truong, P.L., Sim, S.J., 2012. Anal. Biochem. 421, 213–218.
Ilbawi, A.M., Anderson, B.O., 2015. Sci. Transl. Med. 7 278cm1-278cm1.
Jie, G.F., Wang, L., Zhang, S.S., 2011. Chem. – Eur. J. 17, 641–648.
Jun, H.J., Nguyen, A.H., Kim, Y.H., Park, K.H., Kim, D., Kim, K.K., Sim, S.J., 2014. Small 10, 2954–2962.
Ko, Y.J., Maeng, J.H., Ahn, Y., Hwang, S.Y., Cho, N.G., Lee, S.H., 2008. Electrophoresis 29, 3466–3476.
Liu, G., Mao, X., Phillips, J.A., Xu, H., Tan, W., Zeng, L., 2009. Anal. Chem. 81, 10013–10018.
Liu, G.L., Yin, Y., Kunchakarra, S., Mukherjee, B., Gerion, D., Jett, S.D., Bear, D.G., Gray, J.W., Alivisatos, A.P., Lee, L.P., 2006. Nat. Nanotechnol. 1, 47–52.
Lin, M., Chen, C., Shiu, H., Chen, C., Gwo, S., 2009. J. Am. Chem. Soc 131, 10984–10991.
Maruvada, P., Wang, W., Wagner, P.D., Srivastava, S., 2005. Biotechniques, 9–15.
McFarland, A.D., Van Duyne, R.P., 2003. Nano Lett. 3, 1057–1062.
Miwa, M., Nakajima, A., Fujishima, A., Hashimoto, K., Watanabe, T., 2000. Langmuir 16, 5754–5760.
Nguyen, A.H., Sim, S.J., 2015. Biosens. Bioelectron. 67, 443–449.
Niidome, T., Nakashima, K., Takahashi, H., Niidome, Y., 2004. Chem. Commun., 1978–1979.
Niklinski, J., Furman, M., 1995. J. Cancer Prev. 4, 129–138.
Rosi, N.L., Mirkin, C.A., 2005. Chem. Rev. 105, 1547–1562.
Sharmaa, A., Matharua, Z., Sumanaa, G., Solankia, P.R., Kim, C.G., Malhotra, B.D., 2010. Thin Solid Films 519, 1213–1218.
Singh, K.V., Pandey, R.R., Wang, X., Lake, R., Ozkan, C.S., Wang, K., Ozkan, M., 2006. Carbon 44, 1730–1739.
Song, M.S., Choi, S.P., Lee, J.W., Kwon, Y.J., Sim, S.J., 2013. Adv. Mater. 25, 1265–1269.
Truong, P.L., Ma, X., Sim, S.J., 2014. Nanoscale 6, 2307–2315.
Truong, P.L., Cao, C., Park, S.H., Sim, S.J., 2011. Lab Chip 11, 2591–2597.
Waldeisen, J.R., Wang, T., Ross, B.M., Lee, L.P., 2011. ACS Nano 5, 5383–5389.
Wang, G.L., Yu, P.P., Xu, J.J., Chen, H.Y., 2009. J. Phys. Chem. C 113, 11142–11148.
Wang, S., Chen, W., Liu, A., Hong, L., Deng, H., Lin, X., 2012. ChemPhysChem 13, 1199–1204.
Wang, W., Ouyang, H., Yang, S., Wang, L., Fu, Z., 2015. Analyst 140, 1215–1220.
Wei, M., Fang, L., Lee, J., Somu, S., Xiong, X., Barry, C., Busnaina, A., Mead, J., 2008. Adv. Mater. 21, 794–798.
Xue, X.Y., Liu, Y.X., Pan, L., Wang, Y., Wang, K.F., Zhang, M.Y., Wang, P.L., Wang, J.X., 2013. J. Int. Med. Res. 41, 1779–1787.
Yeo, S., Kwon, T., Choi, S., Park, H., Hyun, J.W., Jung, D., 2006. Curr. Appl. Phys. 6, 267–270.
Zhan, Z.R., Ma, X.Y., Cao, C., Sim, S.J., 2012. Biosens. Bioelectron. 32, 127–132.
Zhang, Y., Ma, H., Zhang, K., Zhang, S., Wang, J., 2009. Electrochim. Acta 54, 2385–2391.
Zhang., Y., Liu, W., Ge, S., Yan, M., Wang, S., Yu, J., Li, N., Song, X., 2013. Biosens. Bioelectron. 41, 684–690.
Zhao, J., Zhu, L., Guo, C., Gao, T., Zhu, X.L., Li, G.X., 2013. Biosens. Bioelectron. 49, 329–333.